“Innovative high pressure/high temperature, multi-sensing bioreactors system for microbial risk assessment in underground hydrogen storage”

International Journal of Sciences

Research Article Volume 13 – June 2024 (06)

q-Gaussian and q-BWF Functions Applied to the Decomposition of Pulsar Profiles: Preliminary Results

Amelia Carolina Sparavigna[1]

[1]Department of Applied Science and Technology, Polytechnic University of Turin, Italy

Abstract: The EPN Database of Pulsar Profiles contains data provided by several generous researchers. The data of pulsar profiles are proposed in three different formats. One is the plain text format which allows an easy use of data to test fitting procedures. Literature reports pulsar profile fits made by means of Gaussian line shapes. Here we propose the use of the q-Gaussian functions, which are generalizing the Gaussian functions. Since the observed profiles are also asymmetric, we propose the use for fitting of the q-BWF functions too. These functions are generalizing the Breit-Wigner-Fano line shapes, with the Breit-Wigner factor substituted by the q-exponential function. The q-exponential was proposed by Constantino Tsallis in 1988 for his generalization of Boltzmann-Gibbs statistics. Preliminary fitting examples are here shown, of some profiles from the EPN Database.

Keywords: Pulsar Profiles, Profile Decomposition, q-Gaussian Tsallis Lines, Breit-Wigner-Fano Line Shape, q-BWF Line Shape

Introduction

In a recent study about the radio pulsar emission-beam configurations (Wahl et al., 2023), the researchers used a Gaussian approach to fit the pulsar profiles for recovering the parameters relevant to their geometrical models. The Gaussian fitting procedure was made according to Kramer, 1994, and Kramer et al., 1994. In Wahl et al. and Kramer et al., we find that the pulsar profiles seem consisting of several Gaussian features. Consequently, a relevant problem that we must consider in the pulsar profile analysis is the choice of the method that we use for the decomposition. This is the same problem that we meet in the analysis of the Raman spectra, that is, their decomposition in several spectral components. In the case of Raman spectroscopy, it is well-known that the decomposition depends on the number of components and on the used line-shapes, usually in the form of Lorentzian, Gaussian and Voigt profiles (Ferrari and Robertson, 2000, Meyer, 2005). In 2023, I proposed for Raman spectroscopy a generalization of these profiles in the form of q-Gaussian line shapes. A q-Gaussian is a function based on the Tsallis q-form of the exponential function (Umarov et al., 2008). This generalized exponential is characterized by a q-parameter, and when q is equal to 2, we have the Lorentzian function. If q is close to 1, we have a Gaussian function (this is the reason why this Tsallis function is also known as "q-Gaussian"). For values of q between 1 and 2, we have a bell-shaped function with power-law tails (wings) ranging from the Gaussian to the Lorentzian behavior. As I have shown on many occasions, the q-Gaussian is suitable for fitting Raman spectra in a proper manner (see the discussion proposed in SSRN and the SERS spectra, for instance).

In the case of pulsar profiles, as in the case of Raman spectra, the peaks are often asymmetric. The q-Gaussians, like Gaussian, Lorentzian and Voigt functions, are symmetric. To fit an asymmetric profile, the usual approach is to use more components or to split the line-shape into two parts, characterized by different parameters. For instance, a split-Lorentzian function is a Lorentzian line-shape with independent width parameters for the left and the right parts. However, a different approach to asymmetry exists and it is that based on the Breit-Wigner-Fano line shape. Let us write the BWF(x) function as follow:

$$\mathrm{BWF}(x) = C\frac{\left[1-\xi\gamma^{1/2}(x-x_o)\right]^2}{\left[1+\gamma(x-x_o)^2\right]}$$

When asymmetry parameter ξ is zero, the BWF function becomes a Lorentzian function. Parameter x_o is the center of the line. We can use the q-exponential to generalize the BWF (see also Appendix), and turn BWF into a q-BWF function:

$$q\text{-BWF}(x) = C\left[1-\xi\gamma^{1/2}(q-1)^{1/2}(x-x_o)\right]^2\left[1+(q-1)\gamma(x-x_o)^2\right]^{1/(1-q)}$$

Published at: http://www.ijsciences.com/pub/issue/2024-06/
DOI: 10.18483/ijSci.2768; Online ISSN: 2305-3925; Print ISSN: 2410-4477

Amelia Carolina Sparavigna (Correspondence)
+

Comparing BWF and q-BWF, it is easy to see that the Lorentzian factor is substituted by the q-exponential. Please consider that in literature about Fano resonance (Bianconi, 2003) the parameter ξ is often given by 1/q (with an opposite sign). Here q is indicating the q-parameter related to the Tsallis statistics generalizing the Boltzmann-Gibbs statistics (Tsallis, 1988).

We have obtained good results with q-Gaussians and also with the q-BWF functions in Raman spectroscopy. Confident in the results from spectroscopy, here we start applying the q-Gaussians and the q-BWF functions to the decomposition of the pulsar profiles. The data we consider are from the EPN (European Pulsar Network) Database of Pulsar Profiles, which contains profiles provided by several generous researchers. Data are proposed by means of a web plotting tool. However, the pulsar profiles can be also obtained in the plain text format and therefore they can be easily used to test fit procedures. We could use Gaussian functions, such as in literature, but here we prefer to demonstrate that we can easily use the q-Gaussians for decomposing the pulsar profiles. In the case of evident asymmetry, the q-BWF functions are available too. For showing the decomposition, let us use Fityk software (Wojdyr, 2010). Fityk is a curve fitting and data analysis application, free and open source. It can perform a Levenberg-Marquardt algorithm, among other best fit algorithms. The function of merit is the weighted sum of squared residuals (WSSR), also called chi square. Fityk has several built-in functions but allows to execute a script with user-defined functions (see in the Appendix how we can define in Fityk q-Gaussian, split-q-Gaussian and q-BWF functions).

The aim of the work here proposed is that of investigating deviations from the Gaussian model of the pulsar profile components. The decomposition is the first part of the problem. The second part is that of using the parameters obtained from decomposition into the geometrical specific models (see for instance Wahl and coworkers, 2023). Here we start investigating of the first step: the decomposition by means of q-Gaussians and q-BWF functions. Some preliminary examples regarding profiles from the large database represented by EPN will be given. Before showing decompositions, let us understand how many components we need to use.

Components of the pulsar profiles

A general discussion about pulsars is available in Löwe, 2021, a thesis on the "rotating vector model (RVM) which tries to describe the geometrical properties of pulsars by looking at the polarisation of the arriving signal on Earth". About the physics of the pulsar emission, a review has been proposed by Harding, 2017. "Over the last fifty years since the discovery of pulsars, our understanding of where and how pulsars emit the radiation we observe has undergone significant revision. The location and mechanisms of high-energy radiation are intimately tied to the sites of particle acceleration. The evolution of emission models has paralleled the development of increasingly more sensitive telescopes, especially at high energies" (Harding, 2017).

Different models exist regarding the emission. One of the models is that based on the geometry of core/double cone beams, where two concentric conal beams exist around the central core beam. At p.6 of Joanna Rankin' presentation at Goddard Pulsar Workshop, an image shows how up to five components can be originated in a pulsar profile. In her publication of 2022, Rankin explains that the "Canonical pulsar average profiles are observed to have up to five components (Rankin, 1983). This places an important constraint on the emission-beam topology and underlies the conception of the core/double-cone beam model as originally proposed by Backer (1976)". According to this model, we have two major categories of pulsar profiles, "depending on whether core or conal emission components are dominant at about 1 GHz. Prominent core components occur in single (S_t) profiles consisting of an isolated core component, in core-cone triple (T) profiles with a core component flanked by a pair of outriding conal components, or in five-component (M) profiles where the central core component is flanked by both an inner and outer pair of conal components" (Rankin, 2022). "By contrast, entirely conal profiles include those with a single conal (S_d) component, double profiles (D) consisting of a pair of conal components (occasionally with a weak core component in-between), or conal triple (cT) or quadruple (cQ) profiles where the sightline encounters both conal beams. Outer conal component pairs tend to have an increasing separation with wavelength, whereas inner conal pairs tend to have more constant separations. Also important to these profile classes is single-pulse phenomenology" (Rankin, 2022).

In the work mentioned by Rankin, that is Baker, 1975, we can find the researcher hypothesizing some criteria "for inspecting pulsar radiation". The first is that "The averaged beam pattern is a hollow-cone, perhaps with a pencil beam in the canter, which revolves around the rotation axis. The observer is randomly oriented with respect to the rotation axis at an angle θ_0 and the cone axis is either randomly oriented or randomly aligned with respect to the rotation axis at an angle θ_m. The average waveforms, or profiles, for several observer orientations are given in Figure 1 [by Baker, see here the sketch 1] which gives a schematic of the proposed beam geometry".

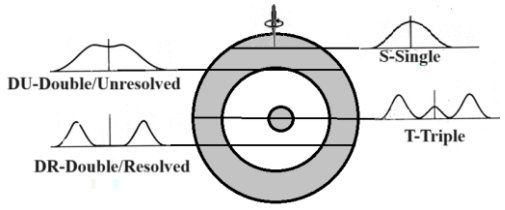

Sketch 1: This sketch is illustrating the Figure 1 in Baker, 1975. In the cone+core model, we have a maximum of three peaks.

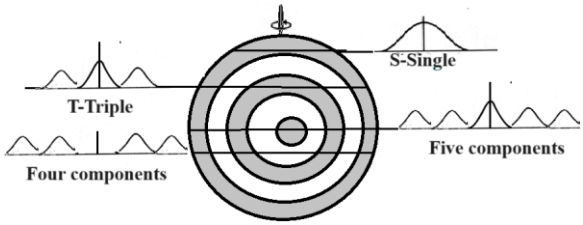

Sketch 2: Here a simple representation of a double-cone+core model. Note please that in the figure in the slide by Rankin, p.6, the distribution in the rings is not depicted as an unbroken whole. It is a "carousel" of subbeams.

Besides the abovementioned model we have also the "patchy" model. That is, according to Beskin and coworkers, 2015, there are "two contrasting phenomenological models to explain the observed pulse shapes". They are shown in Fig. 5 by Beskin et al., 2015. "The 'core and cone' model, proposed by Rankin [Rankin, 1983], depicts the beam as a core surrounded by a series of nested cones. Alternatively, the 'patchy beam' model, championed by Lyne and Manchester [Lyne & Manchester, 1988, Han & Manchester, 2001], has the beam populated by a series of randomly distributed emitting regions. Further work in this area, particularly in trying to quantify the variety of pulse shapes (number of distinct components and the relative fraction that they occur) is necessary to improve our understanding of the fraction of sky covered by the radio pulsar emission beam" (Beskin et al., 2015). Another model, proposed by Wang et al. in 2016, is the Fan Beam Model: "The whole radio beam may consist of several sub-beams, forming a fan-shaped pattern. When only one or a few flux tubes are active, the fan beam becomes very patchy. This model differs essentially from the conal beam models in the respects of beam structure" (Wang et al., 2016).

In Dyks, 2017, it is discussed the cone/core model and proposed a spiral model. "Since the discovery of pulsars in 1967 (Hewish et al.,1968) thousands of pulse profiles have been observed at different radio frequencies ν" (Dyks is mentioning Hankins & Rankin 2010, Mitra et al., 2015, Dai et al., 2015). "Some of the profiles are approximately symmetric, which has led to the nested cone model of the radio emission beam (Ruderman & Sutherland 1975; Backer, 1976; Rankin, 1983)– the main model in use so far. The corresponding emission region consists of two rings and a low-altitude filled-in core region, all centered at the dipole axis and localised at well separated altitudes in pulsar magnetosphere" (see please references given by Dyks, 2017). According to Dyks, 2017, the "model suffers from multiple problems". Among them, we find that "The profiles are often highly asymmetric and have components with flux ratio which curiously evolves with frequency. The latter effect has led to the idea of general patchiness of the beam" (Dyks mentioning Lyne & Manchester 1988; Karastergiou & Johnston 2007). Dyks is also reporting the flux ratio reversal in components, which is observed at different ν, and the existence of "precursor and postcursor components", which "appear on either side of many profiles as additional features" (Dyks, 2017). This is very interesting, because in Raman spectroscopy we find the "shoulders" of the main peaks, which can evolve into separate peaks.

According to the given observations, Dyks proposes a new model: "there exists a geometry which is natural from the point of view of physics, and combines the geometric properties of a cone and a fan beam. It is a flaring spiral (or flaring helix) which makes several revolutions around the dipole axis while the plasma is streaming along this helix towards the light cylinder. When the observer's sightline is traversing through coils of such a spiral, pairs of altitudes are detected, which decrease towards the profile center. This creates the misleading illusion of nested cones, which has been the rule in taxonomical identification of profiles for decades" (Dyks, 2017).

For what is regarding the use of Gaussian profiles, let us consider Wu and Manchester, 1992. "All pulsar emission profiles represent a dynamic superposition of distinct contributions from various emitting regions within the beam. This is the physical basis behind the concept of a component. In many cases, the sight line only sweeps over one individual emission range, or component, such as the conal single profile. *[Wu and Manchester] assumed that the intensity distribution of every component of emission cone is a Gaussian distribution*" (Wu & Manchester, 1992). "For a Gaussian distribution, when the sight line sweeps the emission cone with angle β, the cross section is also a Gaussian distribution". Let us stress that the Gaussian distribution is symmetric, therefore asymmetry needs to be solved with many Gaussian components.

Moreover, (Löwe, 2021), "The signals that are emitted from a pulsar have to travel far to impinge on Earth. These signals get modified in various ways during their voyage to Earth. The reason for these modifications is that the space between the pulsar and Earth is not empty. Instead there are plasmas, gas, dust and magnetic fields. All these are components of the ISM and they modify the signals that are detectable on Earth. The modification of the signals can be described as dispersion, scintillation, scattering and Faraday rotation. All these phenomena impact signals in a different way … [Lorimer and

Kramer, 2012]" (Löwe, 2021).

As previously told, we have the large EPN database to analyze, so let us start giving some preliminary examples of decompositions. In a q-Gaussian distribution, parameter q is characterizing the behavior of its tails (wings). A q-parameter close to 1 tells us that the distribution is Gaussian. Therefore, our approach is relevant for testing the Gaussian character of the pulsar profile components. In the first example, we test also asymmetry.

J1012+5307 - In Dyks et al., 2010, we can find asymmetric profiles. In the Fig.6 by Dyks and coworkers the "main pulse (MP) of a 5.26 ms pulsar J1012+5307 observed at 0.82 GHz (top) and 1.4 MHz (bottom) with the Green Bank Telescope" is given. "The bandwidths were 64 MHz at both frequencies and the total integration time of ∼15 h spanned the period between 2004 July and 2007 March. … The main pulse profile exhibits asymmetry which looks consistent with the" equations proposed in the article by Dyks and coworkers. It seems from the figure that six components had been used for the main component of the pulsar profile.

Let us consider this pulsar in EPN Database. We show the case at 1410.0 MHz, [kxl+98], available link J1012+5307, data courtesy Kramer et al., 1998, EPN database under the Creative Commons Attribution 4.0 International license. The following Figure 1 is a screenshot of Fityk, giving all the peaks of the profile. We have used 6 q-Gaussian functions, three for the main component (see the detail in the Figure 2).

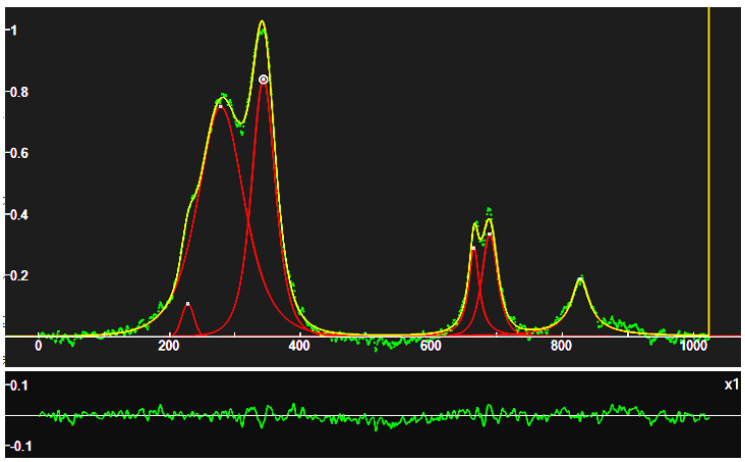

Fig.1: The image is giving a screenshot of Fityk. The data have been fitted to six q-Gaussian functions (red curves). The green dots are representing the data, the yellow line the sum of the components. The lower part of the figure is showing the misfit, that is the difference between data (green) and sum of components (yellow). The q-parameters are, from left to right: 0.99, 1.42, 1.41, 2.06, 1.50 and 2.33.

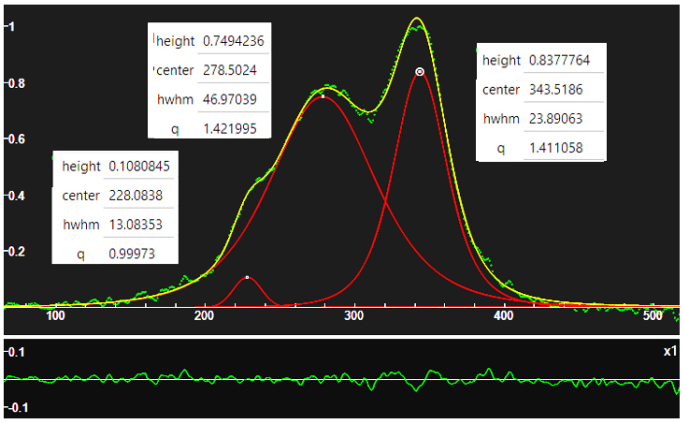

Fig.2: Screenshot of Fityk, giving the decomposition of the main part of the pulsar profile. The parameters of the used three q-Gaussians (red lines) are given in the figure. "hwhm" means "half width at half maximum".

As we can see from the Figure 2, the wings (tails) of the components are quite different from a Gaussian behavior. Only the left small "shoulder" is Gaussian. As we can see from the Figure 1, we have also two over-Lorentzian components, that is profiles with q greater than 2. The misfit is very low. Let us further consider the q-BWF functions. The result is given in the following Fig.3.

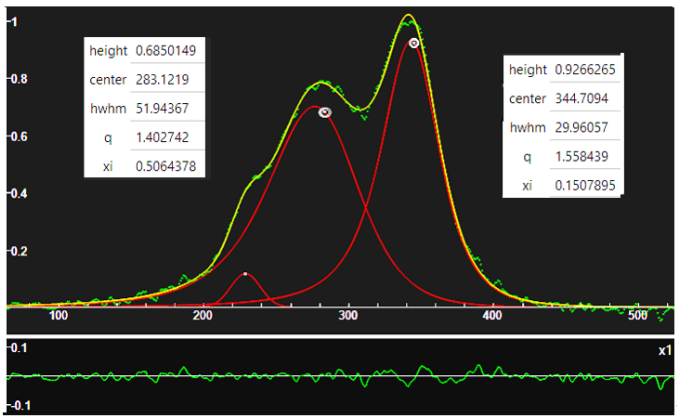

Fig.3: In Fityk, here we used two q-BWFs for the main components. The small shoulder on the left is a q-Gaussian function. Of the q-BWF functions let us note the white encircled points, which are representing the "centers" of the functions. In general, the center of a BWF or q-BWF does not coincide with the position of the peak.

J1133 – To people accustomed to the Raman spectroscopy of biochar, and in general of carbonaceous materials, Figures 2 and 3 remind the D and G bands of the spectrum. Let us see another case, of a profile that reminds a Raman spectrum of graphene oxide. We use two q-BWF functions, because the components look asymmetric. Data are from J1133-6250, 1440 MHz. EPN database under Creative Commons Attribution 4.0 International license. Data courtesy by Guojun and coworkers, 1995.

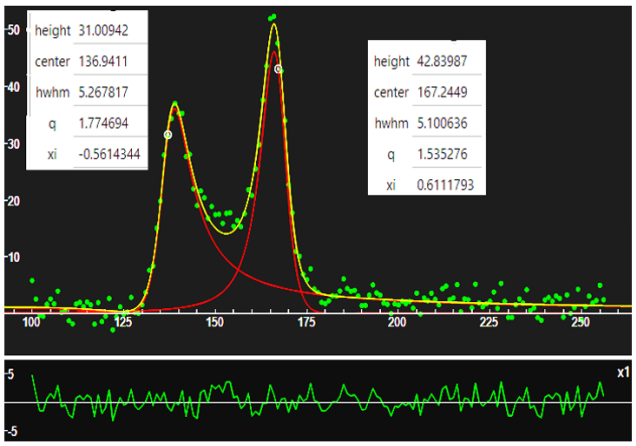

Fig.4: Screenshot of Fityk. The parameters of the two used q-BWFs (red lines) are given in the figure. The sum of the two components is given in yellow, the data in green. Note the two white encircled points. They are representing the "centers" of the q-BWF functions.

In the Figure 4, note that the values of the two q-parameters are 1.54 and 1.77. The functions are far from being of the Gaussian type. The result shown in the Figure 4 is very good, and we have used only two components, that is two q-BWF functions. If we use just two Gaussians or two q-Gaussians, we have a large misfit between the data and the sum of components. Then, we need more than two components to fit the profile. J1133 is considered by Kramer et al., 1994.

J1133 - J1133-6250, 1369 MHz. EPN database under the Creative Commons Attribution 4.0 International license. Data are courtesy by Johnston and Kerr, 2018. Also in this case, let us use two q-BWF functions.

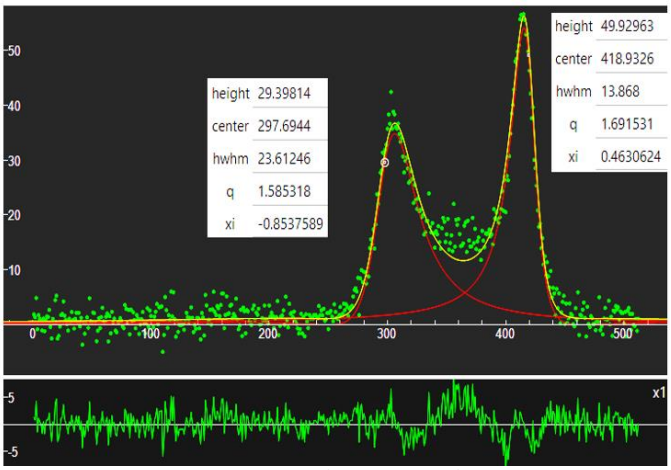

Fig. 5: The data are those of the pulsar profile J1133-6250 (black line). The parameters of the two used q-BWF components (red lines) are given in the figure. Note that the values of the q-parameters are evidencing that the behavior of the functions is not a Gaussian one.

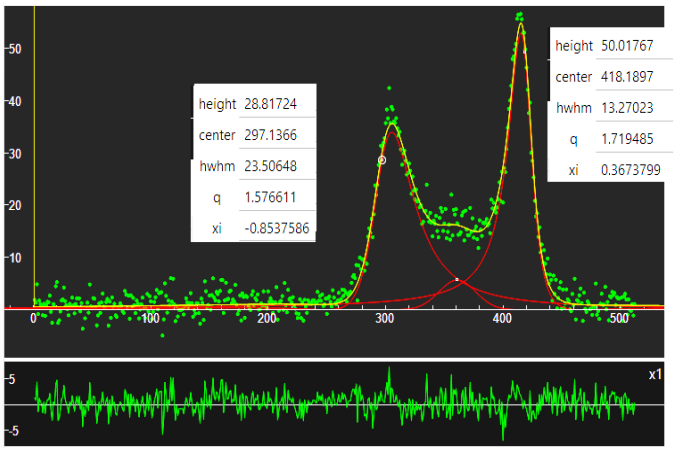

Fig. 6: Data as in the Fig.5. To the two q-Breit functions, a q-Gaussian is added between the peaks. The misfit is reduced.

J1706 - J1706-4310, 1374 MHz. EPN database under the Creative Commons Attribution 4.0 International license. Data are a courtesy by Kramer et al., 2003. Let use two q-Gaussians. Here the result is given in the Fig.7.

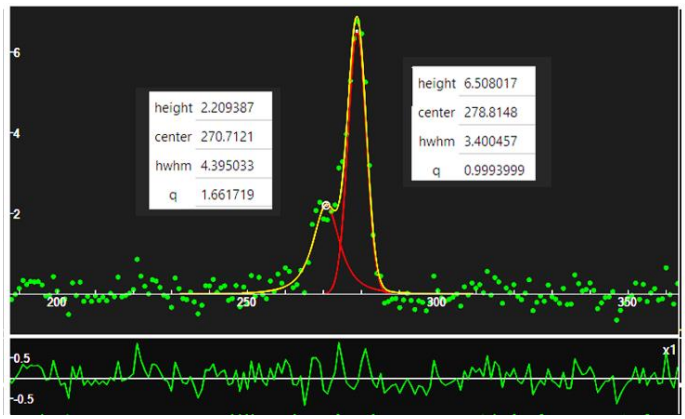

Fig. 7: The data are those of the pulsar profile J1706-4310, 1374 MHz. The parameters of the two q-Gaussians are given in the figure. One, q=0.999, is indicating a Gaussian profile, whereas the other, q=1.662, is telling that the profile is intermediate between Lorentzian and Gaussian line shapes.

J1706 - J1706-3839, 1374 MHz. EPN database under the Creative Commons Attribution 4.0 International license. Data are a courtesy by Kramer et al., 2003. Also in this case, let us use two q-Gaussians.

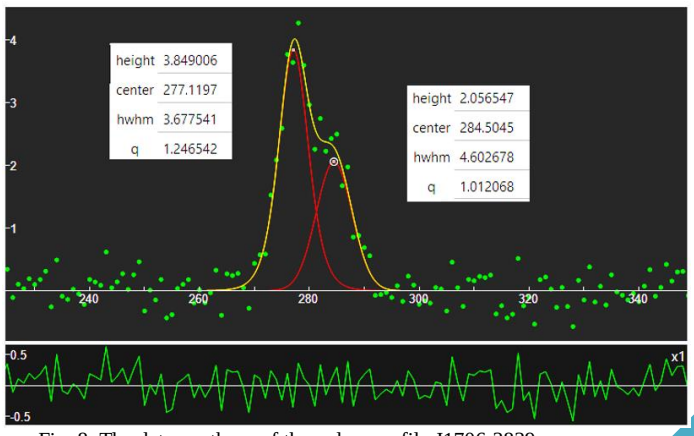

Fig. 8: The data are those of the pulsar profile J1706-3839,

1374 MHz. The parameters of the two used q-Gaussian (red lines) are given in the figure. Note that, in this case, the q parameters are indicating Gaussian-like profiles.

J0435 - J0435+2749, 148.9 MHz. EPN database under the Creative Commons Attribution 4.0 International license. Data are a courtesy by Bilous et al., 2016. In this case we have a large peak which seems being asymmetric.

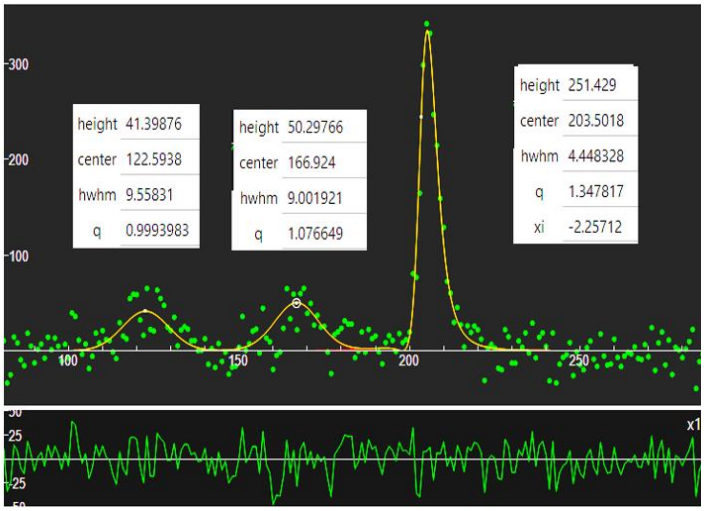

Fig. 9: A profile of J0435+2749, 148.9 MHz. A q-WBF function is used for the main component. Two further q-Gaussians are used as in the figure.

J0435 – Profile of J0435+2749, 337 MHz. EPN database under the Creative Commons Attribution 4.0 International license. Data are a courtesy by Wahl et al., 2023.

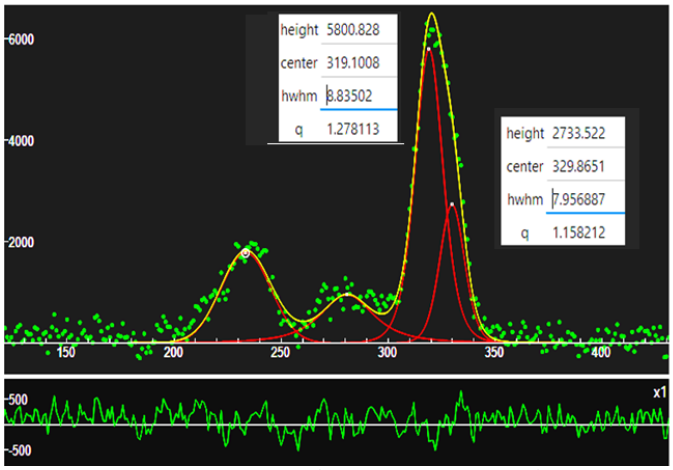

Fig. 10: The same pulsar of the Figure 9, but the profile is given by data J0435+2749, 337 MHz. Four q-Gaussian functions have been used, two are regarding the main peak (the related parameters are given). Note that the values of the q-parameters are close to 1, so we have a Gaussian-like behavior.

J0435 - J0435+2749, 1400 MHz. EPN database under the Creative Commons Attribution 4.0 International license. Data are a courtesy by Wahl et al., 2023. We consider two decompositions. First, we use five q-BWF functions, and then five q-Gaussians.

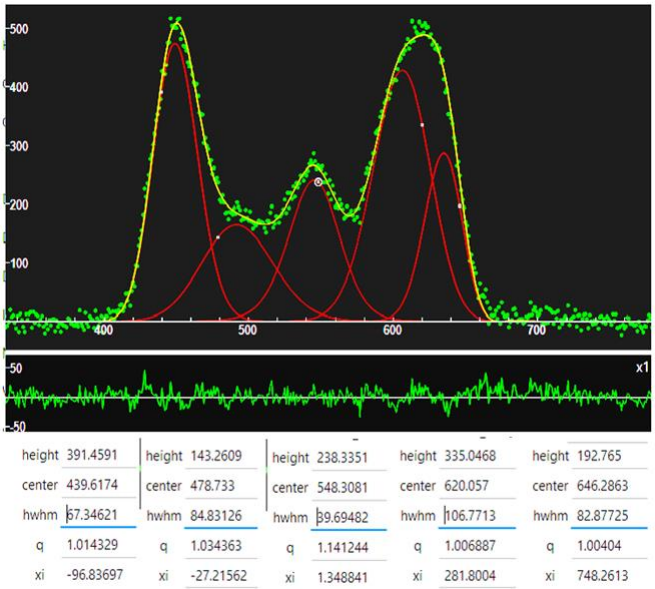

Fig.11: Five q-BWF functions for J0435+2749, 1400 MHz.

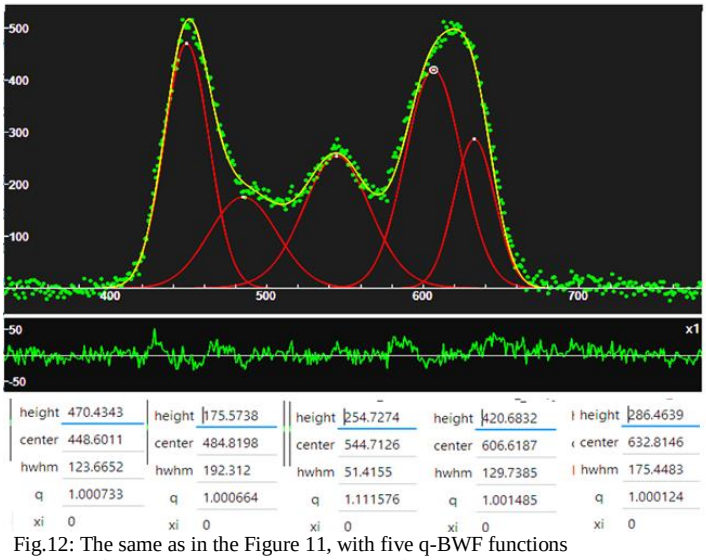

Fig.12: The same as in the Figure 11, with five q-BWF functions with xi fixed to zero. That is, we are using five q-Gaussians.

In the Figure 11, we have shown the decomposition with five q-WBF functions. If we consider the q-parameters, we can see that they are close to the value 1. For this reason, let us fix the value of asymmetry parameter *xi* to zero, in these five functions, and run the Fityk program again. We have the result given in the Figure 12.

Discussion

Figures 11 and 12 are very useful for a discussion regarding the q-BWF functions. As told in the caption of the Figure 3, the center of a q-BWF does not coincide with the position of the peak. The values of "height" and "hwhm", that is "half width at half maximum", are affected by the position of the center, as we can easily see comparing the parameters given in the Figs. 11 and 12. Consequently, the use of q-BWF functions is more complex than that of the q-Gaussians. However, as given by the Figure 4, the q-BWF functions are able of fitting the profiles with a

limited number of components. Further investigation is required, with a systematic analysis of EPN Database of Pulsar Profiles, to determine how many cases need an approach with q-Gaussians instead of Gaussian functions, and of q-BWF asymmetric functions instead of q-Gaussian symmetric functions. Let us stress that the values of the q-parameters can tell us if the pulsar profile features are close to being Gaussian or not.

Notes

About baselines. Only in the case of J1133-6250, a baseline of constant value 40183 has been subtracted from data. No other baseline correction has been applied. 2) The Fityk screenshots show the data as given in the files .txt. Therefore, on the x-axis we have integer values (integer bins). In plots proposed by the EPN Database, a different scale is given. Accordingly, some processing was made by the plotting tool. Let us compare the plot proposed by EPN Database and the plot of data from file .txt in the case of J0435. Using GIMP, the result of comparison is given in the following Figure 13a, where the black curve is representative for data as proposed by the EPN plot and the red curve the data from file .txt. We can see that have a shift. Accordingly, the superposition of the two curves is given in the Figure 13b. Differences are completely negligible.

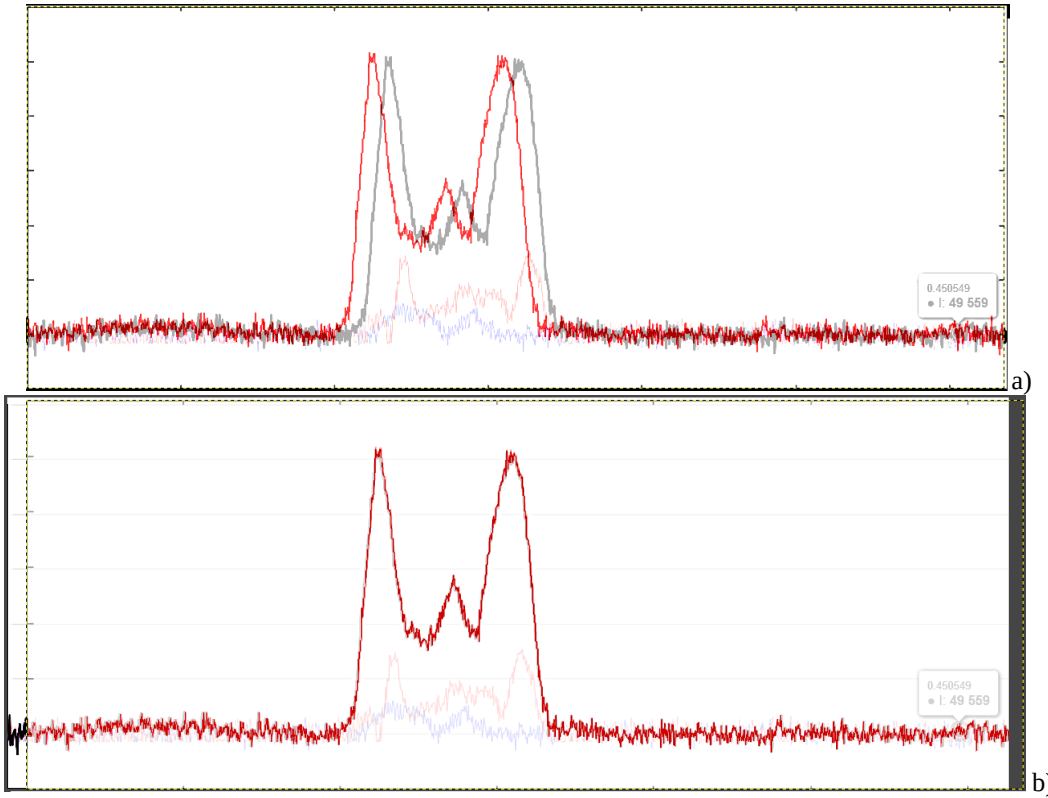

Fig. 13: Panel a): The black curve is representing the data as proposed by the EPN plot and the red curve the data from file .txt. Note the shift. Panel b): The two curves are superimposed.

Appendix – q-Gaussian, split-q-Gaussian and q-BWF functions

The q-Gaussian functions are probability distributions proper of the Tsallis statistics (Tsallis, 1988, Hanel et al., 2009). These functions are based on a generalized form of the exponential function, characterized by a continuous real parameter q. When q is going to 1, the q-exponential becomes the usual exponential function. The value q=2, (Naudts, 2009), corresponds to the Cauchy distribution, also known as the Lorentzian distribution; the q-Gaussian function is therefore a generalization of the Lorentzian distribution too. The change of q-parameter is allowing the q-Gaussian function to pass from the Gaussian to the Lorentzian distribution.

As given by Umarov et al., 2008, the q-Gaussian function is: $f(x) = Ce_q(-\beta x^2)$, where $e_q(.)$ is the q-exponential function and C a scale constant (in the exponent, $\beta = 1/(2\sigma^2)$). The q-exponential has expression: $e_q(u) = [1 + (1-q)u]^{1/(1-q)}$.

To have an asymmetric form of the q-Gaussian function, let us write it in the following manner (the center of the band is at x_o): $q\text{-}Gaussian(x) = Cexp_q(-\beta(x-x_o)^2) = C[1-(1-q)\beta(x-x_o)^2]^{1/(1-q)}$

In ChemRxiv we considered the asymmetric q-Gaussians, as given by Devi (2021):

$q\text{-}Gaussian_L(x) = Cexp_{q_L}(-\beta_L(x-x_o)^2) = C[1-(1-q_L)\beta_L(x-x_o)^2]^{1/(1-q_L)}$, when $x - x_0 <$

0

$q\text{-}Gaussian_R(x) = Cexp_{q_R}(-\beta_R(x-x_o)^2) = C[1-(1-q_R)\beta_R(x-x_o)^2]^{1/(1-q_R)}$, when $x - x_0 > 0$

Parameters q and β of the Left and the Right parts are different. The most proper name for this asymmetric function is split-q-Gaussian. As previously shown, we have also generalized the Breit-Wigner-Fano into a q-Breit-Wigner-Fano.
In Fityk, a q-Gaussian function can be defined in the following manner:

define Qgau(height, center, hwhm, q=1.5) = height*(1+(q-1)*((x-center)/hwhm)^2)^(1/(1-q))
q=1.5 the initial guessed value of the q-parameter. Parameter hwhm is the half width at half maximum of the component. When q=2, the q-Gaussian is a Lorentzian function, that we can find defined in Fityk as:
Lorentzian(height, center, hwhm) = height/(1+((x-center)/hwhm)^2)
When q is close to 1, the q-Gaussian becomes a Gaussian function. The split q-Gaussian is defined as:
Splitqgau(height, center, hwhm1=hwhm, hwhm2=hwhm, q1=1.5, q2=1.5) = x < center ? Qgau(height, center, hwhm1, q1) : Qgau(height, center, hwhm2, q2)

The split Lorentzian is: SplitLorentzian(height, center, hwhm1=hwhm, hwhm2=hwhm) = x < center ? Lorentzian(height, center, hwhm1) : Lorentzian(height, center, hwhm2)
And the q-BWF can be defined as:
Qbreit(height, center, hwhm, q=1.5, xi=0.1) = (1-xi*(q-1)*(x-center)/hwhm)^2 * height*(1+(q-1)^0.5 *((x-center)/hwhm)^2)^(1/(1-q))

And the BWF can be defined as:
Breit(height, center, hwhm, xi=0.1) = (1-xi*(x-center)/hwhm)^2 * height/(1+((x-center)/hwhm)^2)
Using +xi instead of -xi does not change the fitting results in Fityk.

Acknowledgement
Part of this research has made use of the EPN Database of Pulsar Profiles maintained by the University of Manchester, available at https://psrweb.jb.man.ac.uk/epndb/.

References

1. Backer, D. C. (1975). Pulsar average waveforms and hollow cone beam models (No. X-693-75-138). https://ntrs.nasa.gov/api/citations/19750018870/downloads/19750018870.pdf
2. Backer, D. C. (1976). Pulsar average wave forms and hollow-cone beam models. Astrophysical Journal, Vol. 209, p. 895-907.
3. Beskin, V. S., Chernov, S. V., Gwinn, C. R., & Tchekhovskoy, A. A. (2015). Radio pulsars. Space Science Reviews, 191, 207-237. https://doi.org/10.1007/s11214-015-0173-8
4. Bianconi, A. (2003). Ugo Fano and shape resonances. In AIP Conference Proceedings (Vol. 652, No. 1, pp. 13-18). American Institute of Physics.
5. Bilous, A.V., Kondratiev, V.I., Kramer, M., Keane, E.F., Hessels, J.W.T., Stappers, B.W., Malofeev, V.M., Sobey, C., Breton, R.P., Cooper, S., & Falcke, H. (2016). A LOFAR census of non-recycled pulsars: average profiles, dispersion measures, flux densities, and spectra. Astronomy & Astrophysics, 591, p.A134.
6. Dai, S., Hobbs, G., Manchester, R.N., Kerr, M., Shannon, R.M., van Straten, W., Mata, A., Bailes, M., Bhat, N.D.R., Burke-Spolaor, S., & Coles, W.A. (2015). A study of multifrequency polarization pulse profiles of millisecond pulsars. Monthly Notices of the Royal Astronomical Society, 449(3), pp.3223-3262.
7. Devi, S. (2021). Asymmetric Tsallis distributions for modeling financial market dynamics. Physica A: Statistical Mechanics and Its Applications, 578, 126109
8. Dyks, J., Wright, G. A. E., & Demorest, P. (2010). Rotational asymmetry of pulsar profiles. Monthly Notices of the Royal Astronomical Society, 405(1), 509-519.
9. Dyks, J. (2017). The geometry of a radio pulsar beam. Monthly Notices of the Royal Astronomical Society: Letters, 471(1), L131-L134.
10. Fano, U. (1961). Effects of configuration interaction on intensities and phase shifts. Physical review, 124(6), 1866.
11. Ferrari, A. C., & Robertson, J. (2000). Interpretation of Raman spectra of disordered and amorphous carbon. Physical Review B 61: 14095–14107.
12. Guojun, Q., Manchester, R. N., Lyne, A. G., & Gould, D. M. (1995). Polarization and Faraday rotation measurements of southern pulsars. Monthly Notices of the Royal Astronomical Society, 274(2), 572-588.
13. Han, J. L., & Manchester, R. N. (2001). The shape of radio pulsar beams. Mon. Not. R. Astron. Soc, 320, L35-L40.
14. Hanel, R., Thurner, S., & Tsallis, C. (2009). Limit distributions of scale-invariant probabilistic models of correlated random variables with the q-Gaussian as an explicit example. The European Physical Journal B, 72(2), 263.
15. Hankins, T. H., & Rankin, J. M. (2009). Arecibo Multi-Frequency Time-Aligned Pulsar Average-Profile and Polarization Database. The Astronomical Journal, 139(1), 168.
16. Harding, A. K. (2017). Pulsar emission physics: The first fifty years. Proceedings of the International Astronomical Union, 13(S337), 52-57.
17. Hewish, A., Bell, S. J., Pilkington, J. D., Frederick Scott, P., & Collins, R. A. (1979). Observation of a rapidly pulsating radio source. In A Source Book in Astronomy and Astrophysics, 1900–1975 (pp. 498-504). Harvard University Press.
18. Johnston, S., & Kerr, M. (2018). Polarimetry of 600 pulsars from observations at 1.4 GHz with the Parkes radio telescope. Monthly Notices of the Royal Astronomical Society, 474(4), 4629-4636.
19. Karastergiou, A., & Johnston, S. (2007). An empirical model for the beams of radio pulsars. Monthly Notices of the Royal Astronomical Society, 380(4), 1678-1684.
20. Kramer, M., Wielebinski, R., Jessner, A., Gil, J. A., & Seiradakis, J. H. (1994). Geometrical analysis of average pulsar profiles using multi-component Gaussian FITS at several frequencies. I. Method and analysis. Astronomy and Astrophysics Suppl., Vol. 107, p. 515-526 (1994), 107, 515-526.
21. Kramer, M. (1994). Geometrical analysis of average pulsar profiles using multi-component Gaussian FITS at several frequencies. II. Individual results. Astronomy and Astrophysics Suppl., Vol. 107, p. 527-539 (1994), 107, 527-539.
22. Kramer, M., Xilouris, K.M., Lorimer, D.R., Doroshenko, O., Jessner, A., Wielebinski, R., Wolszczan, A., & Camilo, F. (1998). The characteristics of millisecond pulsar emission. I. Spectra, pulse shapes, and the beaming fraction. The Astrophysical Journal, 501(1), p.270.
23. Kramer, M., Bell, J.F., Manchester, R.N., Lyne, A.G., Camilo, F., Stairs, I.H., D'Amico, N., Kaspi, V.M., Hobbs, G., Morris, D.J., & Crawford, F. (2003). The Parkes Multibeam Pulsar Survey–III. Young pulsars and the

discovery and timing of 200 pulsars. Monthly Notices of the Royal Astronomical Society, 342(4), pp.1299-1324.
24. Lorimer, D. R. and Kramer, M. (2012). Handbook of pulsar astronomy, volume 4 of Cambridge observing handbooks for research astronomers ; 4. Cambridge Univ. Press, Cambridge [u.a.].
25. Löwe, N. (2021). Analysing the Rotating Vector Model of Pulsar Radio Emission. Master's Thesis, University of Bielefeld, Faculty of Physics
26. Lyne, A. G., & Manchester, R. N. (1988). The shape of pulsar radio beams. Monthly Notices of the Royal Astronomical Society, 234(3), 477-508.
27. Meier, R. J. (2005). On art and science in curve-fitting vibrational spectra. Vibrational spectroscopy, 2(39), 266-269.
28. Mitra, D., Arjunwadkar, M., & Rankin, J. M. (2015). Polarized quasiperiodic structures in pulsar radio emission reflect temporal modulations of non-stationary plasma flow. The Astrophysical Journal, 806(2), 236.
29. Naudts, J. (2009). The q-exponential family in statistical physics. Central European Journal of Physics, 7, 405-413.
30. Rankin, J. M. (1983). Toward an Empirical Theory of Pulsar Emission-Part Two-on the Spectral Behavior of Component Width. Astrophysical Journal, Vol. 274, NO. 1, P. 359, 1983, 274, 359.
31. Rankin, J. (2016). Observing the Plasma-physical Processes Behind Pulsar Radiation, Goddard Pulsar Workshop, June 2016, available https://fermi.gsfc.nasa.gov/science/mtgs/pulsar_mag/slides/Rankin.pdf
32. Rankin, J. (2022). Radio pulsar beam geometry at lower frequencies: bright sources outside the Arecibo sky. Monthly Notices of the Royal Astronomical Society, 514(3), 3202-3211.
33. Ruderman, M. A., & Sutherland, P. G. (1975). Theory of pulsars-Polar caps, sparks, and coherent microwave radiation. Astrophysical Journal, vol. 196, Feb. 15, 1975, pt. 1, p. 51-72., 196, 51-72.
34. Sparavigna, A. C. (2015). Recurrence plots of pulsar profiles. Philica, 533.
35. Sparavigna, A. C. (2023). q-Gaussian Tsallis Line Shapes and Raman Spectral Bands. Int. J. Sciences, 12(3), 27-40, 2023, http://dx.doi.org/10.18483/ijSci.2671 Available at SSRN: https://ssrn.com/abstract=4398623
36. Sparavigna, A. C. (2023). Asymmetric q-Gaussian functions generalizing the Breit-Wigner-Fano functions. Zenodo. https://doi.org/10.5281/zenodo.8356165
37. Sparavigna, A. C. (2024). The Fitted q-Gaussian Function, from Voigt Profile to Kubo Lineshape. International Journal of Sciences, 13(03), 1-16.
38. Sparavigna, A. C. (2023). SERS Spectral Bands of L-Cysteine, Cysteamine and Homocysteine Fitted by Tsallis q-Gaussian Functions. International Journal of Sciences, 12(09), 14-24.
39. Sparavigna, A. C. (2023). Tsallis q-Gaussian function as fitting lineshape for Graphite Raman bands. ChemRxiv. doi:10.26434/chemrxiv-2023-bwnmw
40. Sparavigna, A. C. (2024). Pyrene and Biochar (Raman Spectroscopy). ChemRxiv. doi:10.26434/chemrxiv-2024-7zbtf
41. Sparavigna, A. C. (2024). Graphene and Graphene Oxide (Raman Spectroscopy). ChemRxiv. doi:10.26434/chemrxiv-2024-86stv-v2
42. Tsallis, C. (1988). Possible generalization of Boltzmann-Gibbs statistics. Journal of statistical physics, 52, 479-487.
43. Umarov, S., Tsallis, C., Steinberg, S. (2008). On a q-Central Limit Theorem Consistent with Nonextensive Statistical Mechanics. Milan J. Math. Birkhauser Verlag. 76: 307–328. doi:10.1007/s00032-008-0087-y. S2CID 55967725.
44. Wahl, H., Rankin, J., Venkataraman, A., & Olszanski, T. (2023). Radio pulsar emission-beam geometry at low frequency: LOFAR High-Band Survey sources studied using Arecibo at 1.4 GHz and 327 MHz. Monthly Notices of the Royal Astronomical Society, 520(1), 314-321.
45. Wang, H.G., Pi, F.P., Zheng, X.P., Deng, C.L., Wen, S.Q., Ye, F., Guan, K.Y., Liu, Y. and Xu, L.Q., 2014. A Fan Beam Model for radio pulsars. I. observational evidence. The Astrophysical Journal, 789(1), p.73.
46. Wojdyr, M. (2010). Fityk: a general-purpose peak fitting program. Journal of Applied Crystallography, 43(5-1), 1126-1128.
47. Wu, X., & Manchester, R. N. (1992). The Intensity Distribution of the Emission Beam and A Discussion of the Radio Luminosity of Pulsars. International Astronomical Union Colloquium, 128, 362–365. doi:10.1017/S0002731600155532